

A comparison of transient heat pump cycle simulations with homogeneous and heterogeneous flow models

Laughman, C.R.; Qiao, H.; Aute, V.; Radermacher, R.

TR2015-072 May 2015

Abstract

This paper compares the effects of two different refrigerant flow modeling assumptions on the transient performance of vapor-compression heat pump cycles. This comparison is done on a dynamic system-level model of a flash tank vapor injection cycle that includes finite volume heat exchanger models. The effect of the flow assumptions and specific slip ratio correlations on both the equilibrium operating point and the transient behavior of the cycle are demonstrated through both simulations and experiments. It is shown that equivalent simulations with different slip ratio correlations each have different equilibrium mass inventories, and that some aspects of the dynamic system behavior, such as the suction superheat or pressure transients, exhibit significant differences both in simulations and in comparison to experimental data.

HVAC+R Research Journal

This work may not be copied or reproduced in whole or in part for any commercial purpose. Permission to copy in whole or in part without payment of fee is granted for nonprofit educational and research purposes provided that all such whole or partial copies include the following: a notice that such copying is by permission of Mitsubishi Electric Research Laboratories, Inc.; an acknowledgment of the authors and individual contributions to the work; and all applicable portions of the copyright notice. Copying, reproduction, or republishing for any other purpose shall require a license with payment of fee to Mitsubishi Electric Research Laboratories, Inc. All rights reserved.

A Comparison of Transient Heat Pump Cycle Models Using Alternative Flow Descriptions

Abstract

This paper compares the effects of two different refrigerant flow modeling assumptions on the transient performance of vapor-compression heat pump cycles. This comparison is done on a dynamic system-level model of a flash tank vapor injection cycle that includes finite volume heat exchanger models. The effect of the flow assumptions and specific slip ratio correlations on both the equilibrium operating point and the transient behavior of the cycle are demonstrated through both simulations and experiments. It is shown that equivalent simulations with different slip ratio correlations each have different equilibrium mass inventories, and that some aspects of the dynamic system behavior, such as the suction superheat or pressure transients, exhibit significant differences both in simulations and in comparison to experimental data.

Introduction

Physically-based dynamic models of vapor-compression heat pump systems are used for a wide variety of purposes, including component design and optimization, system-level design, controls development, and fault detection and diagnostics (FDD), and consequently a wealth of research has examined various classes of these models over the last 30 years (Rasmussen, 2012) (Li, et al., 2014). Such models are generally used for time-domain based simulation, in which the differential equations of the model are integrated forward from some initial condition, and the resulting model dynamics are analyzed to better design, control, or optimize the behavior of the system under study. These so-called white or grey-box models, based upon mathematical models of the physical phenomena, have several appealing characteristics in comparison to alternative black-box approaches, such as neural networks or simplified transfer function models. These advantages include the fact that much of their structure can be formulated by appealing to the basic physical principles, that their creation does not require the *a priori* collection of large amounts of data, and that these models tend to maintain their accuracy over regions of extrapolative use (Cellier, 1991). While

there are many considerations which must be taken into account when constructing such dynamic cycle models, two primary considerations evaluated by the modeler are the selection of the type of heat exchanger model used and the method by which these models are encoded in software and numerically integrated forward in time. Both of these considerations play important roles in the research discussed in this paper.

Heat exchangers usually require particular modeling attention because the timescales over which their behavior evolves are generally much longer than the comparable timescales for the compressors and the expansion devices. In general, there are three main types of heat exchanger models: lumped models, moving boundary models, and distributed parameter models. Lumped heat exchanger models omit the spatial dynamics of the heat exchangers, and are most useful for low-order, fast simulations of the refrigerant-cycle dynamics and the estimation of the system's bulk properties. Moving boundary heat exchanger models describe the spatially averaged dynamics of each of the phasic regions; they are able to capture the spatially-influenced system dynamics significantly better than lumped models, while maintaining a reasonably low model order and a correspondingly fast simulation time. These models can be very useful for developing control algorithms for cycles and systems. Distributed parameter heat exchanger models, such as finite element or finite volume models, are particularly useful for describing spatially dependent phenomena and the detailed component performance, such as the effect of nonuniform air velocities over the surface of heat exchangers, or the branching and joining of refrigerant pipes as a result of particular circuiting configurations.

While the numerical algorithms and methods used to simulate such thermofluid models have traditionally received less attention than their underlying constitutive physical relations, the model implementation and solvers used have a tremendous influence on the accuracy and utility of the resulting simulations. The impact on discretized heat exchanger models is particularly important because the resulting system of equations is not a set of ordinary differential equations (ODEs), but rather a set of differential algebraic equations, or DAEs. DAEs arise in thermofluid systems because of the presence of the algebraic equations of state interrelating the refrigerant properties, such as pressure, temperature, and density. These DAEs are generally harder to solve and integrate than ODEs because the variables in the system must satisfy the algebraic constraints during the integration process. As a result, modeling and

simulation packages which have the capability to operate directly on the set of DAEs are advantageous because of their higher accuracy and usability, in comparison to other packages which rely upon the user to produce a set of ODEs for simulation by manually reducing the index of a set of DAEs by differentiating their algebraic constraints (Brenan, et al., 1989). This index reduction process tends to introduce a high degree of complexity in the resulting sets of ODEs describing the system behavior, producing more coding errors and a lack of flexibility in the use of the models.

Equation-oriented modeling and simulation methodologies (Pantelides & Barton, 1993) that operate directly on the DAEs first became popular in the chemical engineering community and have extended their appeal over the last 20 years. Languages and environments which implement this modeling approach, such as Modelica (Modelica Association, 2014), GPROMs (Process Systems Enterprise, 1997-2014), and Aspen (Aspentech, 2014), use equality statements to directly describe the relations between variables in a model as a set of DAEs, and then use symbolic processing and compiler technology to automatically compile the set of DAEs into a form that can be integrated with a DAE solver, such as DASSL or Radau IIA (Cellier & Kofman, 2006). This approach has been suggestively referred to as behavioral modeling, rather than input-to-output modeling (Willems, 2007), and is particularly applicable to thermofluid systems (Cellier & Kofman, 2006). In particular, the equation-oriented modeling language Modelica has been gaining in popularity for the modeling of complex thermofluid systems (Li, et al., 2014) due to its ability to encode behavioral models into specific objects, which provides the user with a powerful abstraction concept; models can be created that allow different physical effects, such as gravitational head or viscous dissipation, to be easily added or removed. The encoding of models in these environments also has a significant impact on the formulation of the mathematical models, as the models are not constructed with an explicit identification of the inputs and outputs; for example, flowcharts describing the computational order of execution are not relevant in these contexts because the compiler determines the execution causality for a particular simulation with little to no information from the modeler.

Although the decisions pertaining to the heat exchanger discretization and the language of model encoding are perhaps the most important high-level decisions that must be made when creating a dynamic vapor compression cycle simulation, many other modeling choices and decisions will have a significant impact upon the model performance. One such decision is the method for describing the two-phase flow

pattern. A common assumption used in these system models is that both phases flow at the same velocity, otherwise referred to as a homogeneous flow pattern, while the relaxation of this assumption results in different phasic velocities, or a heterogeneous flow pattern (Ghiaasiaan, 2007). While homogeneous flow models are generally reasonable for dispersed flow patterns (e.g., bubbly and spray flow), they are generally not valid for separated flow patterns (e.g., stratified and annular flow) since for these systems (Kolev, 2005),

$$1 \leq S \leq \sqrt{\frac{\rho_L}{\rho_G}} \quad (1)$$

where $S = v_G / v_L$. The choice of flow model used to describe a vapor compression system is important because some of the system's equilibrium characteristics, such as its total mass inventory, are strongly related to the flow regime. One particularly common type of heterogeneous flow model is known as a slip flow model, in which it is assumed that mass transfer across the phasic interface takes place without an accompanying momentum transfer. This model can be formulated as a set of equations describing the two-phase mixture with an extra set of closure relations to relate the different phasic properties to each other, and is consequently much simpler than a complete multifluid model.

Though much of the extant literature describing distributed parameter models of vapor compression systems in Modelica assumes a homogeneous flow model, e.g., (Bonilla, et al., 2012) and (Mortada, et al., 2012), there has been some prior work in using Modelica to develop slip flow models of heat exchangers for vapor compression systems. In (Bauer, 1999), Bauer developed two different slip flow models for the dynamics of an evaporator; one of these models used a static relation to describe the interactions between the phases, while the second model incorporated an innovative description of the mass, momentum, and energy transfer between the phases without developing a complete two-fluid model. These models were validated on a shell-in-tube heat exchanger, with R22 as the working fluid and ethanol as the secondary fluid. The results from this work demonstrated that that the homogeneous flow modeling approach was inadequate to describe the evaporator's mass inventory, and that the performance of the momentum balance with and without a momentum transfer across the two-phase interface were comparable. More recently, (Kaern, 2011) coupled a slip-flow evaporator model to a moving-boundary condenser model and static compressor and expansion valve models to explore and understand the effects of maldistribution in evaporator coils.

Field Code Changed

This slip-flow evaporator model was also compared to a moving boundary evaporator model in (Kaern, et al., 2011), as well as against the performance data from a R22/ethanol heat exchanger.

Other literature that describes transient models of vapor-compression systems, e.g., (Li & Alleyne, 2010), (Kapadia, et al., 2009), and (Ndiaye & Bernier, 2012), does include the use of correlations describing the slip ratio S in their description of the two-phase flow dynamics. These models typically choose a slip correlation based upon a combination of the the correlation's accuracy and its simplicity. However, though a number of slip correlations have been described in the literature, e.g., (Ma, et al., 2009) and (Harms, et al., 2003), each of these correlations is often only compared to the experimentally measured void fraction of either a single heat exchanger or the overall cycle. It thus remains to be seen if the transient behavior of a vapor compression system model is dependent upon the slip correlation used, or if all of the slip correlations yield the same overall system dynamics.

This paper has two principal objectives. First, a set of distributed parameter models of the vapor compression cycle with both homogeneous flow and slip flow models is developed in Modelica. This makes it possible to examine the effect of the flow model on the equilibrium operating point of a closed cycle and better understand and demonstrate the impact of these modeling assumptions on the system dynamics generally and on the distribution of the refrigerant mass specifically. Second, the slip ratio models of (Zivi, 1964), (Smith, 1969), and (Premoli, et al., 1971) are each implemented in otherwise identical versions of the complete cycle model; the resulting comparison of the transients for each of the four transient system models can provide increased understanding of the effect of a specific slip flow model on the overall system dynamics.

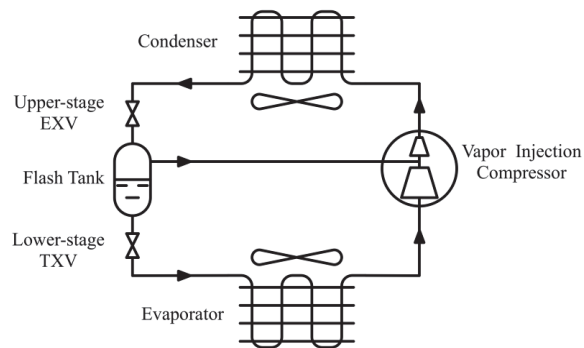


Figure 1: Flash tank vapor injection cycle

Moreover, these different slip models are compared to experimental data for a flash tank vapor injection (FTVI) [heat pump](#) cycle (Qiao, et al., 2015), (Qiao, et al., 2015). The FTVI cycle, illustrated in [Figure 1](#)~~Figure 1~~, was first developed as a means for improving the performance of the simple vapor compression cycle by injecting refrigerant vapor into the compressor, which reduces the compressor discharge temperature and provides a means for adjusting the system capacity. The injection stream is obtained from a flash tank which is located between an upper-stage expansion device that is located after the condenser, and a lower-stage expansion valve that is located before the evaporator. A fraction of the vapor in the flash tank is injected into the compressor, while the remaining liquid refrigerant in the tank enters the lower stage expansion valve. [This study of slip-flow phenomena was particularly relevant to the FTVI low-temperature heat pump cycle because the distribution of refrigerant mass affects the height of the liquid in the flash tank, which can, in turn, have a significant effect on the overall cycle performance. An improved understanding of the refrigerant mass distribution, which is made possible by the slip flow models, can facilitate the construction of more efficient FTVI cycles.](#)

Section 2 of this paper contains descriptions of the component models needed to develop a complete cycle model of an air-to-air heat pump, including a detailed description of the finite control volume models of the heat exchangers. Salient details of the implementation of the slip flow models are then described in Section 3, while Section 4 illustrates a selection of results from the FTVI cycle simulations and experimental data to illustrate the differences between the modeling approaches. Finally, conclusions and potential areas of further exploration are discussed briefly in Section 5.

Model Description

Field Code Changed

Field Code Changed

The construction of a complete cycle model for a simple vapor compression system requires component submodels for the heat exchangers, compressor, and the expansion valve. Due ~~both to~~ both the complexity and the importance of the heat exchanger dynamics to the overall system dynamics, much of this section is focused on these models. Because of the complexity of the two-phase flow model and its associated terminology, the first subsection begins by describing the relations between the phasic and mixture fluid properties in a control volume containing two phases of fluid. The following subsection builds upon these two-phase property and flow relations by describing the construction of a generic control volume model, which contains the set of general fluid conservation relations, the closure relations, and the method by which the spatial dynamics of the thermofluid models are discretized. For the sake of clarity, these control volume models are developed for the assumption of homogeneous flow; the modifications required to describe slip flow will be presented in Section 3. In the final subsection, these dynamic models are used to describe both the refrigerant and air sides of the heat exchanger models. Representative parameter values for the heat exchangers that were used in the experimental apparatus will be described in the Section 4. The other component models, including the compressor, expansion valve, and flash tank, as well as the connection of these component models into the larger cycle models, are also presented in this subsection.

Two-Phase Flow Models

General multiphase flows can be extremely complex because of the potential non-equilibrium conditions for the different phases and the temporally- and spatially-varying transfer of mass, momentum, and energy across the phasic interfaces. A number of simplifications and assumptions were therefore used to make the construction of these models more tractable. These include the assumption of one-dimensional fluid flow, so that the properties are averaged over the flow area, as well as thermodynamic equilibrium within each control volume of the heat exchangers. These assumptions effectively suggest that the flow field containing both phases at a point z_0 is frozen at a point in time, and the spatial average taken over this frozen flow field is also representative of the ensemble average at this point taken over a period of time (Ghiaasiaan, 2007), (Ishii & Hibiki, 2011). Consequently, all of the terms in the following analysis can be taken to be spatially-averaged quantities over the pertinent region.

For a given volume containing two-phase refrigerant in the pipe, an extensive property Ψ can be written as the mass-weighted mixture of the constituent phasic properties by averaging over the phasic volumes, e.g.,

$$\Psi = \Psi_G + \Psi_L \quad (2)$$

$$\psi = \Psi / M_{total} = \psi_g M_g + \psi_L M_L = x\psi_G + (1-x)\psi_L, \quad (3)$$

where x is referred to as the static quality, or

$$x = \frac{M_G}{M_G + M_L} = \frac{M_G}{M_{total}}. \quad (4)$$

The same intensive property ψ can also be written as

$$\psi \rho V = \psi_G \rho_G V_G + \psi_L \rho_L V_L \quad (5)$$

$$\psi \rho = \gamma \psi_G \rho_G + (1-\gamma) \psi_L \rho_L \quad (6)$$

where the void fraction γ can be written as

$$\gamma = \frac{V_G}{V_G + V_L} = \frac{A_G}{A_G + A_L} \quad (7)$$

and the second equality applies when computing the void fraction over a control volume with a fixed length.

These expressions make it possible to write down aggregate intensive properties as a function of their phasic components, either in terms of the void fraction or the static quality, e.g.,

$$\rho = \gamma \rho_G + (1-\gamma) \rho_L \quad (8)$$

$$h = x h_G + (1-x) h_L \quad (9)$$

$$v = x v_G + (1-x) v_L. \quad (10)$$

A relation between the void fraction and the static quality can also be formulated by noting that

$$x = \frac{M_G}{M_{total}} = \frac{\rho_G V_G}{\rho V} = \gamma \frac{\rho_G}{\rho}. \quad (11)$$

Because it will be used in the energy balance, it is also helpful to define a quantity referred to as the flow quality \hat{x} to describe the ratio of the phasic mass flow rates, e.g.,

$$\hat{x} = \frac{\dot{m}_G}{\dot{m}_G + \dot{m}_L} = \frac{\gamma \rho_G v_G}{\gamma \rho_G v_G + (1-\gamma) \rho_L v_L} \quad (12)$$

$$= \frac{x v_G}{x v_G + (1-x) v_L} \quad (13)$$

Equation (12) demonstrates the fact that the static quality is equal to the flow quality only when the gas and liquid velocities are equal. It is also helpful to express the void fraction γ in terms of the flow quality \hat{x} , e.g.,

$$\frac{1}{\gamma} = 1 + \left(\frac{1-\hat{x}}{\hat{x}} \right) \left(\frac{v_G}{v_L} \right) \left(\frac{\rho_G}{\rho_L} \right) \quad (14)$$

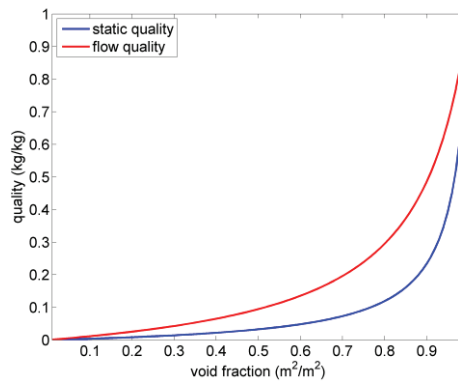


Figure 2: Static quality and flow quality as a function of void fraction, where $\rho_l = 1140 \text{kg/m}^3$, $\rho_v = 38 \text{kg/m}^3$, and the Zivi correlation is used to determine the slip ratio.

The differences between the static quality and the flow quality can also be seen in, where both are plotted as a function of the void fraction.

The states that are chosen for the system are the pressure and the in situ, or density-weighted, enthalpy, based upon the frozen flow field, as defined in Equation (9)(9). This in situ enthalpy differs from the "mixed-cup", or flow-weighted, enthalpy, which is defined as

$$\dot{m} \hat{h} = \dot{m}_G h_G + \dot{m}_L h_L \quad (15)$$

$$\hat{h} = \hat{x} h_G + (1-\hat{x}) h_L \quad (16)$$

Both of these different enthalpies will appear separately in the conservation equations, and are only equal if $x = \hat{x}$.

Control Volume Model

A variety of different conservation and constitutive equations must be established to describe a dynamic model of a refrigerant-to-air heat exchanger. Many of these relations, such as the mass, momentum, and energy balances, apply to both sides of the heat exchanger, while others, such as the closure relations relating the heat transfer to the fluid properties and the temperature difference, or the mass flow to the fluid properties and the frictional pressure drop, are developed for specific fluids and specific geometries. Equations of state which interrelate the fluid properties to each other are also necessary to complete the description of the model, though these will not be discussed in detail here; detailed information about the fluid properties is given in (Elmqvist, et al., 2003) and (McLinden & Klein, 1996). Particular emphasis in this section is placed on the details of the discretization of these underlying PDEs and the construction of the closure relations, as the precise structure of these relations can have a substantial impact on the performance and accuracy of the overall simulation.

As was the case in the previous subsection, a number of assumptions are required to facilitate the process of model construction. These assumptions included the fact that there are no gradients in either the refrigerant properties or the velocity field in the radial or θ directions, that each control volume is in thermodynamic equilibrium, that there is no thermal conduction along either the refrigerant or the heat exchanger wall in the z direction, that the wall temperature in each control volume is uniform, that the change in gravitational potential energy ~~change~~ across the heat exchanger is negligible, and that the dry air medium can be modeled as an ideal gas.

The mass, momentum, and energy balance equations can be written down for an arbitrary single- or two-phase medium by using the two-phase property relations from Section 2.1. These balance equations for each one-dimensional individual control volume can be formulated in a relatively straightforward manner under a homogeneous flow assumption, as discussed in (White, 2008) and (Franke, et al., 2009) are

$$\frac{\partial(\rho A)}{\partial t} + \frac{\partial(\rho Av)}{\partial x} = 0 \quad (17)$$

Field Code Changed

$$\frac{\partial(\rho v A)}{\partial t} + \frac{\partial(\rho v^2 A)}{\partial x} = -A \frac{\partial p}{\partial x} - F_f \quad (18)$$

Field Code Changed

$$\frac{\partial(\rho(u + v^2/2)A)}{\partial t} + \frac{\partial(\rho v(h + v^2/2)A)}{\partial x} = \frac{\partial Q}{\partial x} \quad (19)$$

Field Code Changed

An alternative energy balance (Elmqvist, et al., 2003) can be formulated by multiplying the momentum balance by the fluid velocity v and subtracting it from the original energy balance, resulting in

$$\frac{\partial(\rho u A)}{\partial t} + \frac{\partial(\rho v h A)}{\partial x} = v A \frac{\partial p}{\partial x} + v F_f + \frac{\partial Q}{\partial x} \quad (20)$$

Field Code Changed

This formulation is useful because the only time derivative is that of the internal energy; all other derivatives are spatial. This particular discretization of this PDE will therefore be comparatively easy to express as an ODE, since only derivatives of the internal energy with respect to the state variables are necessary.

The proper state variables with which to describe the balance equations must be chosen for each of these fixed control volumes. The state variables chosen for these models are the pressure p and the *in situ* enthalpy h , since the equation of state for the medium can be represented in these coordinates over the entire thermodynamic space. Expressions for the mass and total internal energy in a given fixed control volume can therefore be written as

$$\frac{d(\rho V)}{dt} = V \left(\frac{\partial \rho}{\partial p} \frac{dp}{dt} + \frac{\partial \rho}{\partial h} \frac{dh}{dt} \right) \quad (21)$$

Field Code Changed

$$\frac{d(u \rho V)}{dt} = \frac{d(\rho h - p)V}{dt} = V \left(\frac{\partial \rho}{\partial p} h - 1 \right) \frac{dp}{dt} + V \left(\frac{\partial \rho}{\partial h} h + \rho \right) \frac{dh}{dt} \quad (22)$$

Field Code Changed

A distinction must be drawn between the above formulation of the balance equations for a element of fluid (Lagrangian reference frame), which has boundaries that can deform over time, and the balance equations for a fixed control volume (Eulerian reference frame), which has stationary boundaries. The balance equations can be converted between the reference frames to formulate the control volume model by using the Reynolds transport theorem,

$$\frac{d\Psi}{dt} = \int_V \frac{\partial(\rho\psi)}{\partial t} dV + \int_A \rho\psi(\vec{v}_B \cdot \hat{n}) dA. \quad (23)$$

Field Code Changed

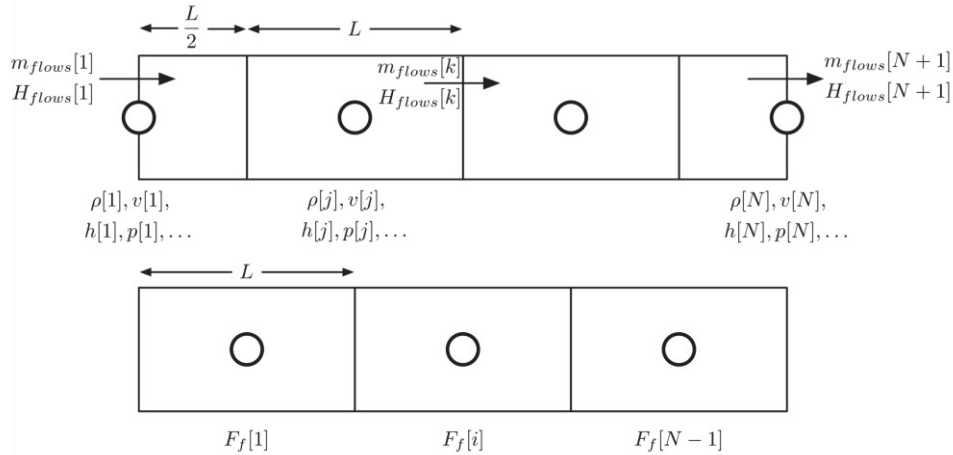


Figure 3: The staggered grids used to solve the balance equations.

The balance equations for fixed control volumes are solved on two staggered grids, as illustrated in [Figure 3](#) ~~Figure 3~~ ~~Figure \ref{fig-staggeredgrids}~~, to avoid the non-physical oscillatory solutions described in (Patankar, 1980). The mass and energy balances are solved on the upper grid, referred to as the thermal grid, while the momentum balance is solved on the lower grid, which is referred to as the momentum grid. This "staggered grid" approach is also helpful because the centers of the upper grids are aligned with the boundaries of the lower grid, so it is not necessary to interpolate properties to find the consistent values on the edges of the momentum grid. Note that there are $i = j - 1$ volumes with j edges on the momentum grid.

The mass balance is only solved on the thermal grid, since all of its variables reside on this grid. Each control volume (CV) of the heat exchanger model will have mass flowing in and out; under the assumption that there are j control volumes and $k = j + 1$ boundaries around those control volumes, and since the mass flow rate of refrigerant across a boundary can be written $m_{flows} = \rho A v$, the mass balance equation can be written as

$$\frac{d(\rho_j V_j)}{dt} = m_{flows,k} - m_{flows,k+1}, \quad (24)$$

Field Code Changed

where the length of integration over the control volume L enters the time derivative on the left hand side, i.e., $V = LA$. The fluid properties, e.g., ρ_j, u_j, p_j , are evaluated in the center of each cell. By explicitly solving for the mass flow rates m_{flows} on each boundary, the practice of evaluating the densities at the boundaries, rather than the middle of the cells, is avoided. Since the fluid properties in the two-phase heat exchangers are C^0 continuous when the pressure and specific enthalpy are the state variables, the changes in density that accompany the changes of state will be implicitly taken into account.

Field Code Changed

The momentum balance equation can be written in a method similar to the mass balance, resulting in

$$\frac{d(m_{flows,i}l)}{dt} = \rho_j v_j^2 A_j - \rho_{j+1} v_{j+1}^2 A_{j+1} + \frac{A_j + A_{j+1}}{2} (p_{j+1} - p_j) + F_{f,i}, \quad (25)$$

Field Code Changed

where the variables with the k index are referred to the edges of the thermal grid cells, the variables with the j index are referred to the centers of the thermal grid cells, and the variables with the i index are referred to the centers of the momentum grid cells. The length of the volume over which equations are solved is denoted l . The friction force $F_{f,i}$ is calculated on the momentum grid because it is related to the mass flow rates $m_{flows,i}$ and the pressure difference between the centers of the adjacent thermal grid $p_{j+1} - p_j$.

The energy balance can also be written for the thermal grid,

$$\frac{\partial(\rho_j u_j A_j)}{\partial t} = H_{flows,k} - H_{flows,k+1} + v_j A_j (p_{j+1} - p_j) + v F_{f,i} + Q_{flows,j}, \quad (26)$$

Field Code Changed

where the values of H_{flows} are also computed at the edges of the control volume using the mass flow rates and the upstream convected mixed-cup enthalpy, e.g.,

$$H_{flows,k} = m_{flows,k} \hat{h}_{upstream,j}, \quad (27)$$

Field Code Changed

and the value of upstream mixed-cup enthalpy is dependent on the flow direction. For the homogeneous flow model, this is identical to the *in situ* enthalpy, but these are not equivalent in the slip flow model. As fluid passes from a two-phase region to a single-phase region, the mixed-cup enthalpy also becomes equal to the *in situ* enthalpy.

One particular aspect in which equation-oriented languages are useful for implementing such models is that they enable the creation of a generic control volume model that can remain otherwise agnostic to the details of the particular higher-level models in which it will be used. By using the principle of inheritance, which is common to many object-oriented languages, a single representation of the conservation equations with a carefully defined interface can be developed, debugged, and then used multiple times without re-implementing the equations. This assists with both the readability and the process of debugging models, as all of the equations representing the underlying physics of the fluid flow are contained in a relatively compact representation and are only coded once. As an example, the number of control volumes used to discretize the heat exchangers, and consequently the number of equations generated in the model, can be adjusted via a single integer parameter in the model. This makes the models easy to customize to particular applications.

In addition to this formulation of the conservation equations, a set of constitutive equations that relate the frictional pressure drop, the heat flow rate, and the slip ratio to other system variables are also needed. While these closure relations are generally constructed from correlations that are developed on the basis of a large set of physical measurements, a naïve implementation of these equations as piecewise functions can cause intractable numerical problems for the solvers due to the discontinuities in the values of either the functions or their derivatives. Smoothness in multiple derivatives (i.e., the classes of C^0 or C^1 functions) is important not only for the integration routine, which may be susceptible to vanishingly small stepsizes or chattering around a discontinuity, but also because the compiler's differentiation of equations for index reduction can impose requirements on the continuity of the derivatives.

An example of the use of techniques to smoothly connect disparate correlations can be seen by considering the construction of a smooth relation between the mass flow rate and the frictional pressure drop. The friction force F_f term included in Equation (18) is equal to the product of the cross-sectional area at location z_0 multiplied by the equivalent frictional pressure drop (Equation (28))

$$\Delta p_{fric} = \zeta \frac{L}{D} \frac{\rho v^2}{2}. \quad (28)$$

The dimensionless friction factor ζ is calculated for flows with $Re < 2000$ by using the Hagen-Poiseuille law (Stephan, 2010), e.g.,

Field Code Changed

$$\zeta_{lam} = \frac{64}{Re}, \quad (29)$$

while the Blasius correlation (Stephan, 2010) for smooth-walled pipes is used for flows with $Re > 6000$, e.g.,

$$\zeta_{urb} = \frac{0.3164}{\sqrt[4]{Re}}, \quad (30)$$

and a cubic polynomial was used to interpolate between these two regions in $\log_{10}(Re)$ vs. $\log_{10}(\zeta)$ coordinates (Elmqvist, et al., 2003) to generate a smooth continuous function ζ for all values of Re . The results of this interpolation can be seen in [Figure 4](#), in which the friction factor for the laminar and turbulent regions are joined by a smooth curve through the transition region. Similar techniques can also be used to create smooth transitions between laminar and turbulent heat transfer coefficients, as well as

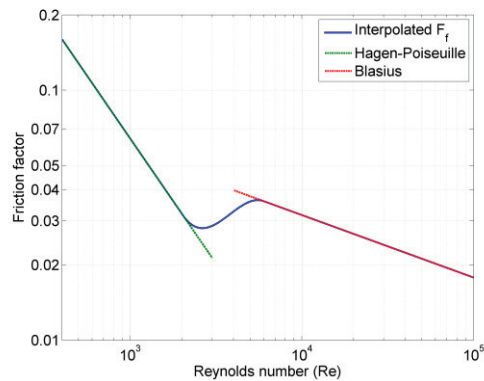


Figure 4: Interpolated smooth Hagen-Poiseuille/Blasius friction factor.

two-phase pressure drop and heat transfer coefficients.

Component and Cycle Models

The construction of the FTVI cycle requires the definition and interconnection of a wide array of components. This section therefore builds first upon the detailed models of the thermofluid flow behavior by creating heat exchanger models which can be used to describe the evaporator and condenser for an complete cycle. A series of other models for the compressor and expansion valve are also briefly discussed

Field Code Changed

Field Code Changed

in this section, before a concluding discussion of the FTVI cycle model under study. These models, as well as models of additional components in the FTVI cycle such as the flash tank and the thermostatic expansion valve, are adapted from those used in (Qiao, et al., 2015); the reader is referred to that reference for more detailed information about these models.

Field Code Changed

Because the type of physical interactions between the fluid and its local environment are common to both the refrigerant side and the air side of the heat exchanger, the control volume model can be used to describe the fluid behavior on both sides of the heat exchanger. The control volumes for each side of the heat exchanger are defined with different heat transfer coefficients and pressure drop correlations; the correlations and constant values used for each heat exchanger are provided in [Table 1](#)~~Table 1~~. In addition, the air side of the heat exchanger uses a moist-air model, allowing the description of both sensible and latent heat transfer on the coil. The conservation equations in each control volume are thus solved to determine whether dehumidification occurs on a given section of the coil, as well as the amount of mass transfer that occurs.

Name	Correlation
Air side forced convection heat transfer and pressure drop (dry)	(Wang, et al., 1999)
Air side forced convection heat transfer and pressure drop (wet)	(Wang, et al., 2000)
Refrigerant side single-phase heat transfer	(Stephan, 2010)
Refrigerant side single-phase pressure drop	(Stephan, 2010)
Refrigerant side condensing heat transfer	(Shah, 1979)
Refrigerant side condensing pressure drop	(Lockhart & Martinelli, 1949)
Refrigerant side evaporating heat transfer	(Kandlikar, 1990)
Refrigerant side evaporating pressure drop	(Gronnerud, 1979)

Table 114: Correlations used for the heat exchangers

The governing heat transfer equations for the air side [describing both sensible and latent heat transfer](#) are

$$\dot{m}_{air} c_{p,air} \frac{dT_{air}}{dy} \Delta y = \alpha_{air} (A_{o,tube} + \eta_{fin} A_{o,fin}) (T_w - T_{air}) \quad (31)$$

$$\dot{m}_{air} \frac{d\omega_{air}}{dy} \Delta y = \alpha_m (A_{o,tube} + \eta_{fin} A_{o,fin}) \min(0, \omega_{water,sat} - \omega_{air}) \quad (32)$$

where $\omega_{water,sat}$ is the humidity ratio of the air calculated at the wall temperature and the fin efficiency η_{fin} is calculated using the equation proposed by (Hong & Webb, 1996). The mass transfer coefficient α_m is calculated by using the Lewis analogy

$$\alpha_m = \frac{\alpha_{air}}{c_{p,air} Le^{2/3}} \quad (33)$$

where $Le^{2/3} = 0.9$ (Kuehn, et al., 1998).

The refrigerant wall is modeled as one-dimensional heat conduction in the direction perpendicular to the refrigerant flow, with convective boundary conditions described by the refrigerant-side and air-side heat transfer coefficients. This wall element can be modeled simply as a one node thermal capacitance by

$$(m_w c_w + m_{fin} c_{fin}) \frac{dT_w}{dt} = \alpha_{ref} A (T_r - T_w) + \dot{m}_{air} [c_{p,air} (T_{air,in} - T_{air,out}) + (\omega_{air,in} - \omega_{air,out}) \Delta h_{fg}] \quad (34)$$

In creating the models for the condenser and the evaporator, the abstractions afforded by the object-oriented paradigm can be utilized by creating both component models as instances of a generic heat exchanger model. For example, the condenser model can be created by first instantiating a heat exchanger model and then modifying this particular instance to reflect the characteristics of the particular application. Such modifications might include the inclusion of specific geometric parameters, particular heat transfer or pressure drop correlations, or circuiting patterns. This ability to create a generic model and then modify specific instances makes it possible to create robust and reliable models which accurately describe the underlying physics of the fluid flow, yet which are flexible enough to use in a variety of applications.

A simple isenthalpic model of the expansion valve is used to describe the expansion process, which has neither mass nor energy storage. The mass flow rate through the expansion device is related to the size

of the orifice in the valve θ , as well as the density at the inlet of the valve ρ_{in} and the pressure drop across the valve $P_{in} - P_{out}$, e.g.,

$$\dot{m}_{EV} = \theta \sqrt{\rho_{in} (P_{in} - P_{out})}. \quad (35)$$

The FTVI cycle includes 2 expansion devices: an electronic expansion valve (EXV) and a thermostatic expansion valve (TXV). The refrigerant side of both devices use the simple orifice model presented in Equation (35), but the means of controlling the orifice size in the devices differs considerably; the EXV is controlled by a PID control loop with gains that are selected by the system designer, while the TXV is controlled through a mechanical feedback loop.

The model of the scroll compressor with an injection port is quite complex, owing to the dependence of the flow direction through the injection port on the intermediate pressure. This model is based upon the thermodynamics of the physical compression process, rather than the conventional AHRI 540 compressor map; this model was used because it has improved ability to describe the compressor performance at points other than those used to fit the model parameters (Jahnig, 2000). The general structure of the compressor with the injection port is illustrated in Figure 5.

Formatted: Indent: First line: 0"

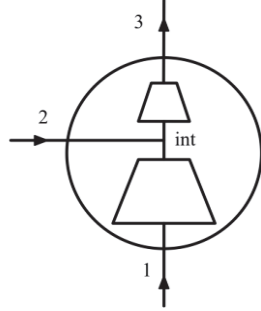


Figure 5: Diagram of compressor with injection port

The simulation of the compression process will be described below, though the full compressor model also describes the heat transfer from the motor, the control volumes present at the inlet and outlets, and so forth (Qiao, et al., 2015). The refrigerant flow rate through the scroll set of the compressor is given by

$$\dot{m}_1 = \left[a_1 + a_2 \left(\frac{p_2}{p_1} \right)^{\frac{1}{n}} \right] \rho_1 V_{disp} \frac{N}{60} \quad (36)$$

where the constants a_1 , a_2 , and the polytropic index $n = 1.35$ are determined through a compressor performance test. The refrigerant flow rate through the injection port is given by

$$\dot{m}_2 = \text{sign}(p_2 - p_{int}) a_3 \sqrt{\rho_{int} |p_2 - p_{int}|} \quad (37)$$

where *sign* indicates the use of the signum function and $p_{int} = \zeta^n p_1$ is the intermediate internal pressure after the first compression stage, under the assumption of a polytropic compression process and a first stage volume ratio $\zeta = 1.21$.

The refrigerant temperature after the first compression stage is given by

$$T_{int} = T_1 \left(\frac{p_{int}}{p_1} \right)^{\frac{n}{n-1}} \quad (38)$$

while the refrigerant enthalpy after the two streams mix is given by

$$h_{mix} = \begin{cases} \frac{\dot{m}_1 h_{int} + \dot{m}_2 h_2}{\dot{m}_1 + \dot{m}_2} & \text{for } p_2 - p_{int} > 0, \\ h_{int} & \text{for } p_2 - p_{int} \leq 0, \end{cases} \quad (39)$$

Field Code Changed

The refrigerant temperature after the entire compression process is given by

$$T_3 = T_{mix} \left(\frac{P_3}{P_{int}} \right)^{\frac{n-1}{n}} \quad (40)$$

and the discharge mass flow rate is determined by

$$\dot{m}_3 = \frac{\sqrt{\rho_3(P_3 - P_{int})}}{f_{dis}} \quad (41)$$

where the discharge port pressure drop coefficient f_{dis} is also determined experimentally.

The dynamic model of the flash tank is also quite complex, due to the dependence of the flow regime on the height of the liquid level in the tank with respect to the outlet port. The governing equations for the flash tank can be described by

$$V_{FT} \frac{d\bar{\rho}_{FT}}{dt} = \dot{m}_in - \dot{m}_{liq,out} - \dot{m}_{vap,out}$$

$$V_{FT} \left(\bar{\rho}_{FT} \frac{d\bar{h}_{FT}}{dt} - \frac{d\bar{p}_{FT}}{dt} \right) = \dot{m}_in (h_{in} - \bar{h}_{FT}) - \dot{m}_{liq,out} (h_{liq,out} - \bar{h}_{FT}) - \dot{m}_{vap,out} (h_{vap,out} - \bar{h}_{FT})$$

where the specific enthalpy of the refrigerant leaving the flash tank is dependent on the whether the refrigerant in the tank is two-phase ($h_f < \bar{h}_{FT} < h_g$) or if it is single phase ($\bar{h}_{FT} < h_f$ or $\bar{h}_{FT} > h_g$)
sta. Additional details regarding this model are provided in (Qiao, et al., 2015).

Model Implementation

In principle, the system of mixture equations discussed in Section 2 describes the thermofluid dynamics for both homogeneous flow and slip flow, where the slip flow model also contains an additional closure relation that defines the slip ratio in terms of other thermodynamic variables. In practice, however, such an implementation is not computationally effective, because of the discontinuities between the single phase and two-phase regions. For example, the calculation of the slip ratio v_G / v_L will go to infinity in the superheated region; this will either cause problems with numerical robustness, elicit the development of complex techniques to activate or deactivate particular equations, or some combination thereof.

Two alternative formulations of the slip flow closure relations that have improved numerical behavior were evaluated in this work. In the first of these approaches, the mean fluid velocity v and the phasic velocity difference Δv are used to describe the slip between the different phases, while the second

Formatted: MTDisplayEquation

Field Code Changed

Field Code Changed

Field Code Changed

Field Code Changed

approach uses the difference between the flow enthalpy and the *in situ* enthalpy, referred to as the correction enthalpy h_c , to improve the numerical performance of the simulation. Each of these formulations will be discussed in turn.

The first of these approaches to address these discontinuities was proposed in (Bauer, 1999), in which the mean velocity v and the velocity difference Δv are used to calculate the balance equations, rather than the phasic velocities. This is done by using the expression for the mixture velocity (Equation (10)) to formulate an expression for the phasic velocities, e.g.,

$$v_G = v + (1-x)(\Delta v) \quad (42)$$

$$v_L = v - x(\Delta v) \quad (43)$$

This makes it possible to express the phasic mass flow rates in terms of v and Δv ,

$$\dot{m}_G = \gamma \rho_G v_G A \quad (44)$$

$$= xv\rho A + x(1-x)(\Delta v)\rho A \quad (45)$$

$$= x\dot{m} + \dot{m}_{corr} \quad (46)$$

$$\dot{m}_L = (1-x)\dot{m} - \dot{m}_{corr}, \quad (47)$$

where $\dot{m}_{corr} = x(1-x)(\Delta v)\rho A$, and is calculated at the centers of each element of the thermal grid, as are all of the other thermodynamic properties. This can also be used to develop the following relation between x and \hat{x} ,

$$\hat{x} = x + x(1-x)\frac{\Delta v}{v}. \quad (48)$$

This reformulation of the phasic velocities is particularly useful because the term proportional to Δv goes to zero both when $x \leq 0$ and when $x \geq 1$.

The balance equations can be rewritten by using these expressions; the correspondingly reformulated mass balance for a fixed control volume is

$$\frac{dM}{dt} = \dot{m}_{G,in} + \dot{m}_{L,in} - \dot{m}_{G,out} - \dot{m}_{L,out} \quad (49)$$

$$\frac{d(\rho_j V_j)}{dt} = m_{flows,k} - m_{flows,k+1}, \quad (50)$$

while the modified momentum balance for the fixed control volume can be written as

$$\frac{dI}{dt} = \dot{I}_{in} - \dot{I}_{out} + (P_{in} - P_{out})A + F_f \quad (51)$$

$$\frac{d(m_{flows,i}I)}{dt} = \rho_j v_j^2 A_j + \dot{m}_{corr,j}(\Delta u)_j - \rho_{j+1} v_{j+1}^2 A_{j+1} - \dot{m}_{corr,j+1}(\Delta u)_{j+1} + \frac{A_j + A_{j+1}}{2}(p_{j+1} - p_j) + F_{f,i}, \quad (52)$$

where $I = m_{flows} l$. Finally, the energy balance for the fixed control volume can be rewritten as

$$\frac{dU}{dt} = \dot{m}_{in} \hat{h}_{in} - \dot{m}_{out} \hat{h}_{out} + vA(P_{in} - P_{out}) + vF_f + \dot{Q} \quad (53)$$

$$\frac{d(\rho_j u_j A_j)}{dt} = H_{flows,k} - H_{flows,k+1} + v_j A_j (p_{j+1} - p_j) + vF_{f,i} + \dot{Q}_{flows,k} \quad (54)$$

where H_{flow} is again computed using the mixed-cup enthalpy, rather than the *in situ* enthalpy. While the mass and energy balances appear to be identical to the homogeneous flow mixture equations, the phasic velocities will differ due to the non-unity slip ratio.

While this implementation of the slip flow equations works well for correlations in which the slip ratio is explicitly calculated as a function of other thermodynamic variables (e.g., Zivi or Premoli), the equations relating the phasic velocities to the other variables of interest become more complex when using a void-fraction correlation instead of a slip ratio correlation. Since the slip ratio is implicitly provided by the correlation in such cases, the Modelica compiler must manipulate the set of equations in the model to solve for all of the variables; as a result, the compiler must sometimes solve a nonlinear set of simultaneous equations at each integration step. Though such conditions can sometimes be resolved by manipulating the set of equations (e.g., Equation (14)) into a more suitable form, alternative solutions to this problem are desirable.

Consequently, an alternative slip flow formulation was proposed in (Qiao, et al., 2015) and is designed to be more suitable for the use of void-fraction correlations. Rather than characterize the flow dynamics with the mean velocity v and the velocity difference Δv , this method uses the *in situ* enthalpy h and an enthalpy correction term Δh_c to describe the slip phenomenon. This enthalpy correction term is defined as

$$\Delta h_c = \hat{h} - h \quad (55)$$

$$\Delta h_c = (\hat{x} - x)(h_g - h_f) \quad (56)$$

Formatted: Font: Italic

Field Code Changed

This formulation facilitates the use of void fraction formulations that directly calculate the flow quality \hat{x} . Rather than working with an implicit relationship between the void fraction and the slip ratio, the use of the enthalpy correction term makes it possible to first calculate \hat{x} from the void fraction correlation, and then use the knowledge of x , h_f and h_g to calculate h_c and \hat{h} in turn. Moreover, the set of discretized equations does not have to be modified from those used for the homogeneous model because \hat{h} is computed directly without the modification of other terms.

This method has two significant features, the first of which is that the terms relating to the phasic velocities will not blow up during transitions between single-phase and two-phase regions. Unlike the slip ratio, Δh_c is well-behaved in that the transition between the single and two-phase zones is smooth, and it also goes to zero outside of the two-phase region. In addition, void fraction correlations with implicit relations between the slip ratio and the flow quality can also be used more reliably.

It is important to note that numerical instabilities can still arise when using this second method with particular slip ratio or void fraction correlations. As explicit slip ratio correlations, such as that defined by (Premoli, et al., 1971), often have a very nonlinear relation between the slip ratio and the flow quality, the compiler must either rearrange the equations when defining the order of execution or iteratively solve for the flow quality as a function of the other variables. Such problems can arise when there are implicit and/or nonlinear relationships between groups of variables.

The above analysis suggests that the choice of the slip flow implementation must generally be matched with the slip ratio or void fraction correlation being used. Each of these implementations represents an improvement over the explicit calculation of the slip ratio, which goes to infinity as the liquid velocity goes to zero. In general, equation-oriented modeling languages are well suited to this type of investigation because the different slip ratio models can be individually replaced in the overall cycle model without changing any of its other behavioral characteristics. Despite the power of these languages, however, the compilers cannot solve high-index nonlinear sets of DAEs in their full generality, and care must be taken during the model construction to ensure that the compiler will be able to generate a model that can be accurately integrated.

To evaluate the efficacy of both of these implementations for simulating slip flow in vapor compression cycles, the (Zivi, 1964), (Smith, 1969), and (Premoli, et al., 1971) slip flow correlations were implemented in the system dynamic model. These correlations are given in [Table 2](#), [Table 2](#),

Name	Correlation
(Zivi, 1964)	$S = \left(\frac{\rho_g}{\rho_f} \right)^{-1/3} \quad (5758)$
(Smith, 1969)	$S = K + (1-K) \left[\frac{\frac{\rho_f}{\rho_g} + K \left(\frac{1-\hat{x}}{\hat{x}} \right)}{1 + K \left(\frac{1-\hat{x}}{\hat{x}} \right)} \right]^{1/2} \quad (5859)$ <p>$K = 0.4$</p>
(Premoli, et al., 1971)	$S = 1 + F_1 \left[\frac{y}{1 + yF_2} - yF_2 \right]^{1/2}$ $F_1 = 1.578 \text{Re}_{\text{fo}}^{-0.19} \left(\frac{\rho_f}{\rho_g} \right)^{0.22}$ $F_2 = 0.0273 \text{We}_{\text{fo}} \text{Re}_{\text{fo}}^{-0.51} \left(\frac{\rho_f}{\rho_g} \right)^{-0.08} \quad (5960)$ $y = \frac{\hat{x}\rho_f}{(1-\hat{x})\rho_g}$ $\text{Re}_{\text{fo}} = \frac{\rho_f v D}{\mu_f}$ $\text{We}_{\text{fo}} = \frac{\rho_f v^2 D}{\sigma}$

Table 22: Slip flow correlations evaluated in this paper

where Re_{fo} and We_{fo} are calculated under the assumption that only liquid is traveling through the channel.

Results

A set of dynamic models of the complete flash tank vapor injection cycle were constructed to explore the system behavior by interconnecting the component models developed in the previous sections. These models were used to explore two main aspects of the system dynamics. First, the behavior for the model with the homogeneous flow assumption is compared to the behavior with the slip flow assumption. The

cycle behavior utilizing the different slip flow correlations is then explored to characterize the effect of specific slip flow assumptions on the transient cycle dynamics.

The impact of the flow assumptions on a variety of system variables are therefore explored in this work. First, the effect of the different correlations on the steady-state system charge, and more particularly on the evaporator charge, are described. This is followed by the study of dynamic performance of the cycle with variation in the slip flow parameters. Some of the system variables that are unobservable from experimental observations, such as the slip ratio or the static quality, are studied first; this is followed by a comparison of the simulations to data collected from an experimental FTVI system that is described in detail in (Qiao, et al., 2015). Such a comparison will be developed both for the system behavior during a startup transient as well as for transients that deviate from a steady-state operating point.

The models described above were implemented using the Modelica compiler Dymola 2015 (Dassault Systemes, 2014) and tested extensively on a set of FTVI cycle models that used fluid models for moist air and R410a which are included in the commercially available Air-Conditioning Library (Modelon AB, , 2014). [A representative simulation of the transient behavior of the cycle over a 600 second time horizon ran on an 3.4 GHz Intel Core-i7 64-bit machine with 8 Gb of RAM in 373 seconds.](#) Each of these models is identical except for relations used to describe the slip ratio in the heat exchangers. These models were each initialized from the same set of starting pressures and air-side temperatures to ensure a valid basis for

Field Code Changed

Input Parameter	Value
Condenser inlet air temperature	21.1 degrees C [70 degrees F]
Condenser inlet relative humidity	75%
Evaporator inlet air temperature	8.3 degrees C [45 degrees F]
Evaporator inlet relative humidity	48%
System refrigerant charge	7.0 kg [15.4 lbm]
Compressor speed	3500 rpm

comparison, listed in ~~Table 3~~ ~~Table-3~~. The ~~resulting~~ mass inventories for these models ~~after this~~ ~~initialization step for the thermal states~~ are listed in ~~Table 4~~ ~~Table-4~~.

It is evident from the data presented in ~~Table 4~~ ~~Table-4~~ that there are significant differences between the evaporator mass inventory of the different cycles, and that these differences are responsible for the majority of the discrepancy between the complete cycle mass inventories. More specifically, the slip flow cycles had a total evaporator inventory that is 75-85% higher than the homogeneous flow cycle, though the cycles were all initialized at the same operating point. These differences in charge are due in part to the fact that the liquid phase velocity is much lower than the vapor phase velocity, causing the total residence time of the liquid in the heat exchangers to be much longer for the slip flow cycles than for the homogeneous flow cycle. However, these differences in charge between the cycles with the different flow assumptions are only relevant to the components' two-phase flows; since many of the components in the cycle have single phase flow, the influence of the slip ratio is not manifest ~~in these components, and the charge inventory for these single phase components will be the same for all of the cycles. The mass inventory in the condenser is also quite similar, because much of the mass is contained in the subcooled section of the condenser, and because the length of the two-phase region in the condenser is shorter than it is in the evaporator. These differences in refrigerant mass would have likely been even larger if the refrigerant dissolved in the oil taken into account, but such refrigerant/oil multicomponent fluid modeling was not developed in this work.~~

Slip Ratio Correlation	Evaporator Mass Inventory	Condenser Mass Inventory	System mass inventory
Homogeneous model	275 g [9.70 oz]	1532 g [54.0 oz]	5374 g [189.6 oz]
(Zivi, 1964)	498 g [17.6 oz]	1570 g [55.4 oz]	5672 g [200.1 oz]
(Smith, 1969)	483 g [17.0 oz]	1555 g [54.9 oz]	5627 g [198.5 oz]
(Premoli, et al., 1971)	509 g [18.0 oz]	1567 g [55.3 oz]	5679 g [200.3 oz]

Table 44: Mass inventories for simulations with different slip ratios

Turning to the transient cycle behavior, one set of simulations is illustrated in [Figure 8](#), [Figure 6](#), and [Figure 7](#) to illustrate the differences between these the cycle models with the different flow assumptions. At t=50 seconds during this experiment, the expansion valve stroke fraction

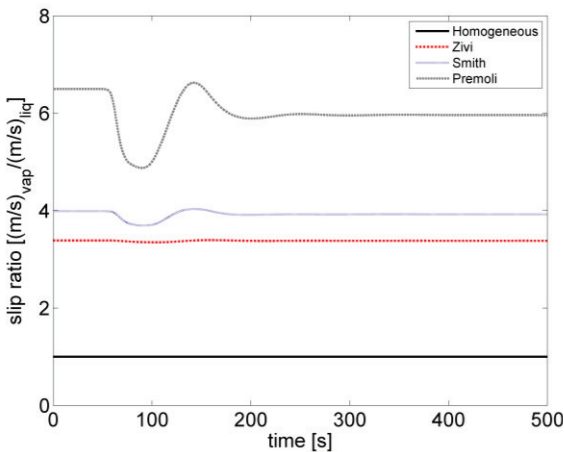


Figure 7: Slip ratio in the middle of the evaporating section for all of the cycle models during a transient step in the expansion valve orifice size

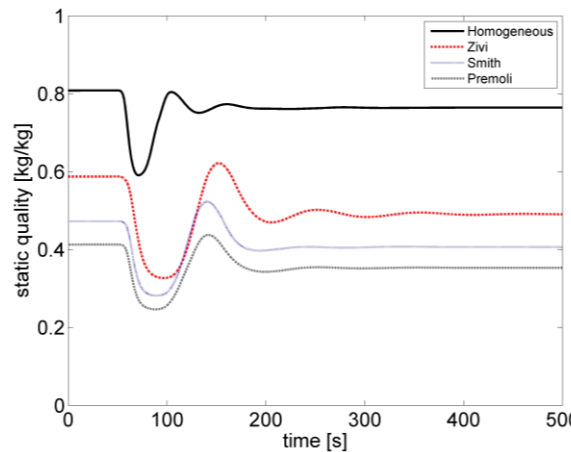


Figure 6: Static quality in the middle of the evaporating section for all of the cycle models during a transient step in the expansion valve orifice size

was increased from 22% to 25%.

[Figure 8](#) and [Figure 6](#) demonstrate the effect of the different slip ratios on the transient

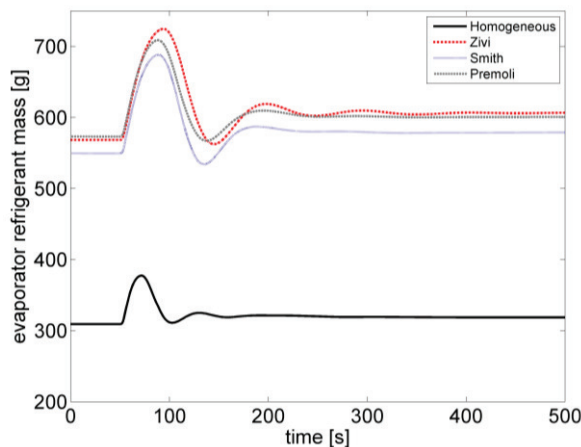


Figure 8: Evaporator mass inventories for all cycle models during a transient step in the expansion valve orifice size.

response of the system. In particular, it is clear from ~~Figure 8~~ that both the magnitude and the duration of the transient response of the evaporator mass inventory for the homogeneous cycle are smaller than the equivalent responses for the slip flow models. It is also interesting to note that the different slip flow correlations correspond to different transient responses; the response of the simulation in which the Zivi correlation is implemented is more underdamped than the response of the model with the Premoli correlation. More information about the system response in these conditions is also provided in ~~Figure 6~~, which illustrates the time-varying slip ratio in the heat exchangers at one point in the middle of the condensing section. The slip ratio for the Premoli cycle is approximately twice the value of that for the Zivi cycle, and the slip ratio transient for the Premoli cycle also has much more variation than the slip ratio for the Zivi cycle. One possible explanation for the different amounts of damping is that the higher slip ratios of the Smith and Premoli cycles cause a stronger coupling between the slip ratio and other cycle dynamics than for the Zivi and homogeneous cycles. This may cause the dynamic responses of the homogeneous and Zivi cycles to be qualitatively similar, though the magnitude of the evaporator mass inventories are different. However, an examination of the static quality dynamics at the same point, illustrated in ~~Figure 7~~, suggest that comparable differences are not found in all of the dynamics; the dynamics of the static quality for all of the three slip flow simulations are qualitatively similar, and are significantly slower than the dynamics for the single phase flow.

While these simulation studies revealed the potential for new understanding of the dynamic system behavior, it was also important to experimentally validate the trends observed in these simulations. The results of these simulations were therefore also compared to experimental data collected on an FTVI system which incorporated a wealth of sensors that could be used to analyze and optimize the cycle. Particularly salient characteristics of this heat exchangers in the experimental platform are collected in Table 5: additional ~~Detailed~~ information about the experimental FTVI platform can be found in (Qiao, et al., 2015). Data collected on the experimental system was compared both to the transients from a steady-state operating point, in the same manner as the previous plots, as well as to the startup transients of the machine.

<u>Parameter</u>	<u>Outdoor coil</u>	<u>Indoor coil</u>
------------------	---------------------	--------------------

Field Code Changed

Formatted Table

<u>Tube length</u>	<u>2565 mm [101.0 in]</u>	<u>483 mm [19.0 in]</u>
<u>Tube outer diameter</u>	<u>7.9 mm [0.311 in]</u>	<u>9.5 mm [0.374 in]</u>
<u>Tube wall thickness</u>	<u>0.8 mm [0.0315 in]</u>	<u>0.8 mm [0.0315 in]</u>
<u>Tubes per bank</u>	<u>32</u>	<u>26</u>
<u>Number of tube banks</u>	<u>2</u>	<u>3</u>
<u>Coils in parallel</u>	<u>1</u>	<u>2</u>
<u>Fin type</u>	<u>Louver fin</u>	<u>Louver fin</u>
<u>Air mass flow rate</u>	<u>1.18 kg/s [156.1 lbm/min]</u>	<u>0.70 kg/s [92.6 lbm/min]</u>

Table 5: Selected parameters of experimental platform

Formatted: Keep with next

Formatted: Caption

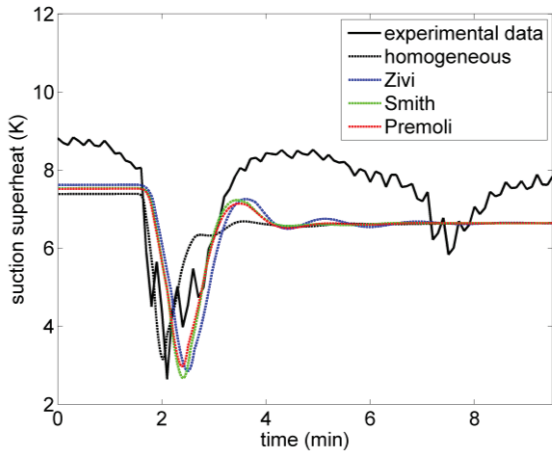


Figure 12: Compressor suction superheat temperature for both experiment and simulation

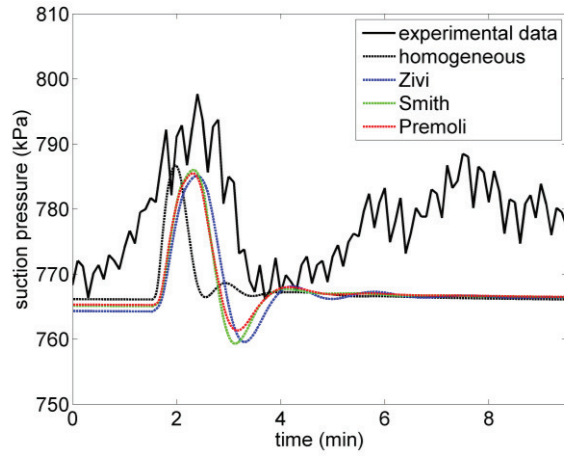


Figure 11: Suction pressure for both experiment and simulation.

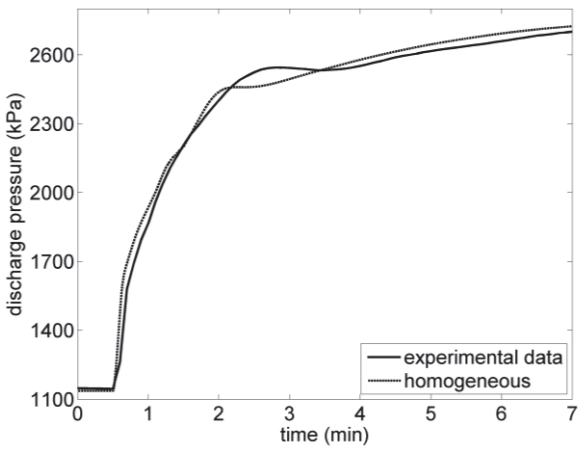


Figure 10: Suction pressure for both experiment and homogeneous flow simulations of the startup transient.

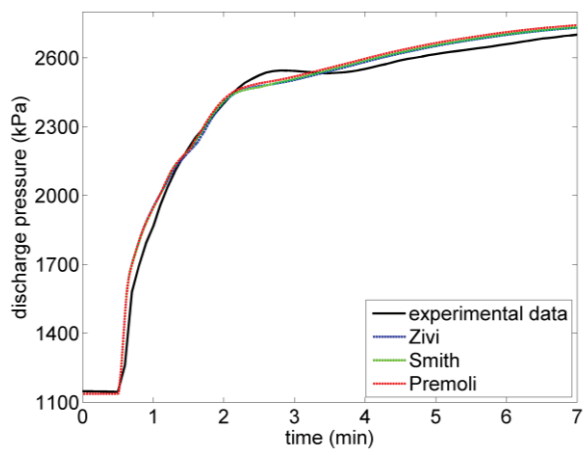


Figure 9: Discharge pressure for experiment and slip flow simulations of the startup transient.

The overall importance of including a model of slip flow in the heat exchangers can be clearly seen from the plots illustrated in [Figure 11](#) and [Figure 12](#), though there are some discrepancies between the experimental data and the simulation data due in part to inaccuracies in the TXV model. [During this experiment, the system was perturbed from the steady-state operating point described by the parameters listed in Tables 4 and 5 by stepping the high-pressure electronic expansion valve from a stroke fraction of 22% to 25%, while leaving all other control inputs constant.](#) Looking first at the suction superheat data illustrated in [Figure 12](#), the transient corresponding to the homogeneous flow

assumption is much faster than both the experimental data and the comparable slip flow transients. This phenomenon is likely due to the greater inertia of the liquid component of the flow. The suction pressure

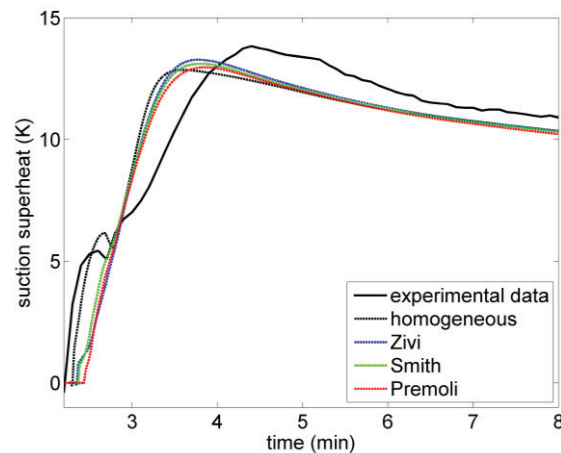


Figure 13: Superheat temperature for both experiment and simulations of startup transient.

data illustrated in [Figure 11](#)[Figure 14](#) also shows similar dynamics, in that the transients corresponding to the slip flow simulations resemble the experimentally collected waveforms much more closely than do the homogeneous flow simulations. These results suggest that modeling the slip ratio in heat exchanger models is important to accurately describe the dynamic behavior of the system.

A comparison of the startup transients of the experimental data and the simulations yields results that are somewhat different than the steady-state transients, as can be seen in [Figure 13](#)[Figure 13](#), [Figure 9](#)[Figure 9](#), and [Figure 10](#)[Figure 10](#). In general, all of the startup waveforms are very similar, suggesting that the impact of the flow model on the startup transient is not as great as the impact on steady-state transients. In comparing the minor differences, however, it appears that the homogeneous flow model captures the system dynamics more accurately during the startup transient than the slip flow models do. For example, the discharge pressure transients in both the experimental data and the homogeneous flow model that are illustrated in [Figure 10](#)[Figure 10](#) are more underdamped than the slip flow transients illustrated in [Figure 9](#)[Figure 9](#). Moreover, only the homogeneous flow transient reproduces the clear discontinuous excursion in [Figure 13](#)[Figure 13](#) that is evident in the experimental data, unlike the slip flow transients. It is likely that these differences can be attributed to the fact that the fluid immediately after

startup is homogeneous, and takes some time to develop into either a boiling or condensing flow after the compressor is turned on.

Conclusions and Future Work

A heterogeneous slip flow model for two-phase heat exchangers was proposed in this paper, and a Modelica implementation of a complete models of a flash-tank vapor injection cycle with different flow assumptions was discussed. In addition, the output of these models was compared to experimentally collected data on the FTVI cycle. In comparing the characteristics of these cycle models, it is clear that the slip flow cycle models have a significantly higher evaporator mass inventory than the homogeneous model, and that the timescale of the steady-state transients observed in the experimental data matches the output of the slip flow models more closely than that of the homogeneous flow models. It is also notable that the startup transients are generally very similar, suggesting that the use of a heterogeneous flow model is not as significant during the initial startup transient, and that the homogeneous flow model might be more valid during this startup period. On the basis of these results, it is clear that the some of the differences between the cycles with either homogeneous flow or slip flow are not negligible, and that the flow model must be carefully considered when developing models, especially those which will be calibrated to experimental data. These considerations are especially pertinent to cycles in which the total refrigerant charge is minimized, as the portion of the cycle which contains two-phase refrigerant is considerably greater than in cycles with large superheated or subcooled volumes. Future work should include additional experimental validation to further characterize the differences between startup and steady-state transient behavior to create a flow model that can be used in both the startup and steady-state regimes.

Nomenclature

A	cross-sectional area	k	Thermal conductivity	i, j, k	Control volume index
D	Tube diameter	\dot{m}	Mass flow rate	dis	Discharge port
F	Force	p	Pressure	suc	Suction port
I	Momentum	u	Specific internal energy	G	Gas
L	Wall thickness	v	Velocity	L	Liquid
M	Mass	x	Static quality	b	Bulk
Q	Heat flow rate	\hat{x}	Flow quality	$corr$	Correction
S	Slip ratio = v_G / v_L	α	Heat transfer coefficient	a, air	Air
T	Temperature	γ	Void fraction	$w, wall$	Wall
U	Internal energy	ζ	Friction factor	f	Friction factor
V	Volume	η	Efficiency		
c	Specific heat capacity	ρ	Density		
h	<i>In situ</i> specific enthalpy	θ	EXV stroke fraction		
\hat{h}	“mixed-cup” specific enthalpy	Ψ	Extensive property		
ω	Humidity ratio	ψ	Intensive property		

Bibliography

- Aspentech, 2014. *Aspen HYSYS*. s.l.:s.n.
- Bauer, O., 1999. *Modeling of Two-Phase Flows in Modelica*, s.l.: s.n.
- Bonilla, J., Yebra, L. & Dormido, S., 2012. Chattering in dynamic mathematical two-phase flow models. *Applied Mathematical Modeling*, Volume 36, pp. 2067-2081.
- Brenan, K., Campbell, S. & Petzold, L., 1989. *Numerical Solution of Initial Value Problems in Differential Algebraic Equations*. s.l.:North Holland (republished by SIAM).

Cellier, F., 1991. *Continuous System Modeling*. s.l.:Springer-Verlag.

Cellier, F. & Kofman, E., 2006. *Continuous System Simulation*. s.l.:Springer.

Dassault Systemes, A., 2014. *Dymola*. s.l.:s.n.

Elmqvist, H., Tummescheit, H. & Otter, M., 2003. *Object-oriented modeling of thermo-Fluid systems*. s.l., s.n.

Franke, R. et al., 2009. *Stream connectors: An extension of {M}odelica for device-oriented modeling of convective transport phenomena*. s.l., s.n.

Franke, R. et al., 2009. *Standardization of thermo-fluid modeling in {M}odelica.{F}luid*. s.l., s.n.

Ghiaasiaan, S., 2007. *Two-Phase Flow, Boiling, and Condensation in Conventional and Miniature Systems*. s.l.:Cambridge University Press.

Gronnerud, R., 1979. Investigation of liquid hold-up, flow resistance and heat transfer in circulation type evaporators, part IV: Two-phase flow resistance in boiling refrigerants. *Annexe 1972-1, Bull. de l'Inst du Froid, International Institute of Refrigeration*.

Harms, T., Groll, E. & Braun, J., 2003. Accurate charge inventory modeling for unitary air conditioners. *HVAC&R Research*, 9(1), pp. 55-78.

Hong, K. & Webb, R., 1996. Calculation of fin efficiency for wet and dry fins. *HVAC&R Research*, 2(1), pp. 27-41.

Ishii, M. & Hibiki, T., 2011. *Thermo-Fluid Dynamics of Two-Phase Flow*. 2 ed. s.l.:Springer.

Jahnig, D. a. R. D. a. K. S., 2000. A semi-empirical method for representing domestic refrigerator/freezer compressor calorimeter data. *ASHRAE Transactions*, 106(2), pp. 1-9.

Kaern, M., 2011. *Analysis of flow maldistribution in fin-and-tube evaporators for residential air-conditioning systems*. s.l.: s.n.

Kaern, M., Elmegaard, B. & Larsen, L., 2011. *Experimental comparison of the dynamic evaporator response using homogeneous and slip flow modeling*. s.l., s.n.

Kandlikar, S., 1990. A general correlation for saturated two-phase flow boiling heat transfer inside horizontal and vertical tubes. *Journal of Heat Transfer*, Volume 112, pp. 219-228.

Kapadia, R., Jain, S. & Agarwal, R., 2009. Transient characteristics of split air-conditioning systems using {R}22 and {R}410A as refrigerants. *HVAC&R Research*, 15(3), pp. 617-649.

Kolev, N., 2005. *Multiphase Flow Dynamics 2*. s.l.:Springer.

Kuehn, T., Ramsey, J. & Threlkeld, J., 1998. *Thermal Environmental Engineering*. 3 ed. s.l.:Prentice Hall.

Li, B. & Alleyne, A., 2010. A dynamic model of a vapor compression cycle with shut-down and start-up operations. *International Journal of Refrigeration*, 33(3), pp. 538-552.

Li, P. et al., 2014. Recent advances in dynamic modeling of {HVAC} equipment. {P}art 2: Modelica-based modeling. *HVAC&R Research*, 20(1), pp. 150-161.

Li, P. et al., 2014. Recent advances in dynamic modeling of {HVAC} equipment. {P}art 1: Equipment modeling. *HVAC&R Research*, 20(1), pp. 136-149.

Lockhart, R. & Martinelli, R., 1949. Proposed correlation of data for isothermal two-phase, two-component flow in pipes. *Chemical Engineering Progress Symposium Series*, Volume 45, pp. 39-48.

Ma, X. et al., 2009. Experimental validation of void fraction models for {R}410a air conditioners. *International Journal of Refrigeration*, Volume 32, pp. 780-790.

McLinden, M. & Klein, S., 1996. *A next generation refrigerant properties database*. s.l., s.n.

Modelica Association, 2014. *Modelica Specification, Version 3.3*. s.l.:s.n.

Modelon AB, , 2014. *Air Conditioning Library User Guide*, s.l.: s.n.

Mortada, S., Zoughaib, A., Clodic, D. & Arzano-Daurelle, C., 2012. Dynamic modeling of an integrated air-to-air heat pump using {M}odelica. *International Journal of Refrigeration*, 35(5), pp. 1335-1348.

Ndiaye, D. & Bernier, M., 2012. Transient model of a geothermal heat pump in cycling conditions - Part {A}: The model. *International Journal of Refrigeration*, 35(8), pp. 2110-2123.

Pantelides, C. & Barton, P., 1993. Equation-oriented dynamic simulation: Current status and future perspectives. *Computers and Chemical Engineering*, 17(S1), pp. S263-S285.

Patankar, S., 1980. *Numerical Heat Transfer and Fluid Flow*. s.l.:Hemisphere Publishing Co..

Premoli, A., Francesco, D. & Prina, A., 1971. A dimensional correlation for evaluating two-phase mixture density. *La Termotecnica*, Volume 25, pp. 17-26.

Process Systems Enterprise, 1997-2014. *gPROMS*. s.l.:s.n.

Qiao, H., Aute, V. & Radermacher, R., 2015. Transient modeling of a flash tank vapor injection heat pump system - Part I: Model development. *International Journal of Refrigeration*, Volume 49, pp. 169-182.

- Qiao, H., Xu, X., Aute, V. & Radermacher, R., 2015. Transient modeling of a flash tank vapor injection heat pump system - Part II: Simulation results and experimental validation. *International Journal of Refrigeration*, Volume 49, pp. 183-194.
- Rasmussen, B., 2012. Dynamic modeling for vapor compression systems. Part 1: Literature review. *HVAC&R Research*, 18(5), pp. 934-955.
- Shah, M., 1979. A general correlation for heat transfer during film condensation inside pipes. *Int. J. Heat Mass Transfer*, Volume 22, pp. 547-556.
- Smith, S., 1969. Void fractions in two-phase flow: A correlation based upon an equal velocity head model. *Proc. Inst. Mech. Eng.*, Volume 184, pp. 647-664.
- Stephan, P., ed., 2010. *VDI Heat Atlas*. s.l.:Springer-Verlag.
- Wang, C., Lee, C., Chang, C. & Lin, S., 1999. Heat transfer and friction correlation for compact louvered fin-and-tube heat exchangers. *International Journal of Heat and Mass Transfer*, Volume 42, pp. 1945-1956.
- Wang, C., Lin, Y. & Lee, C., 2000. Heat and momentum transfer for compact louvered fin-and-tube heat exchangers in wet conditions. *International Journal of Heat and Mass Transfer*, Volume 43, pp. 3443-3452.
- White, F., 2008. *Fluid Mechanics*. 6th ed. s.l.:McGraw-Hill.
- Willems, J., 2007. The behavioral approach to open and interconnected systems. *IEEE Control Systems Magazine*, Volume 27, pp. 46-99.
- Zivi, S., 1964. Estimation of steady-state steam void fraction by means of the principle of minimum entropy production. *J. Heat Transfer*, Volume 86, pp. 247-252.